Proper Orthogonal Decomposition Based Control of Transverse Beam Vibrations: Experimental Implementation [1]

R.C.H. del Rosario[2], H.T. Tran[3] and H.T. Banks[4]
Center for Research in Scientific Computation
Box 8205, North Carolina State University
Raleigh, NC 27695-8205

Abstract

LQG compensator control of transverse vibrations was implemented on an aluminum cantilevered beam in a "smart structure" paradigm. The beam was mounted with two self-sensing, self-actuating piezoceramic patches. The Euler-Bernoulli beam equation was discretized via a Galerkin type approximation (referred to as the full order model). To reduce the size of the resulting finite dimensional approximating system, the Proper Orthogonal Decomposition (POD) was employed as a reduced basis method. A reduction of dimension from 34 to 2 was obtained through the model reduction technique. Feedback control based on the reduced order system was implemented in real time using a dSpace DS1103 control system. Experimental results indicate that POD based control achieves comparable control attenuation with full order model based control.

1 Introduction

Real-time control of smart material structures requires numerical integration of the linear system at each discrete time step at which the real-time processor runs. For complex structural systems such as shells [16, 17, 18] or structural acoustic systems [6], the computationally intensive algorithms needed for the online computation of PDE-based controls must be supplemented by model reduction techniques. Numerical studies in [5] have shown the feasibility of employing model reduction techniques in feedback control of thin cylindrical shells perturbed by a periodic external force. This investigation provides the next step in the development of efficient model based feedback control methodologies by implementing the ideas presented in [5] in a physical system. We chose to demonstrate the ideas in the context of a beam system but the extension of the ideas to more complex systems is rather straightforward.

The proliferation of the use of the Proper Orthogonal Decomposition (POD) as a

[1]Research supported in part by the U.S. Air Force Office of Scientific Research under grants AFSOR F49620-95-1-0236 and AFSOR F49620-98-1-0180, and in part by the National Science Foundation grant DUE-9751284

[2]email:rcdelros@math01.cs.upd.edu.ph

[3]email:tran@control.math.ncsu.edu

[4]email:htbanks@eos.ncsu.edu

reduced basis method in control and estimation applications can be attributed to its ability to accurately represent the system data with only a small number of basis elements (or POD modes). The system data obtained at different parameter values can either be experimental measurements of the state or numerical simulations of the system. The POD method attempts to extract characteristic information from the data through an orthogonalization procedure. It is essentially a linear transformation of a multivariate data set into an optimal set of uncorrelated variables or POD modes. Approximation applications of POD include turbulent coherent flows [3, 12, 13, 27, 38, 20], structures [30, 31, 32, 33, 35], materials processing [24, 23, 29, 28, 41], characterization of human faces [39], and statistical and pattern recognition fields [19], to name a few. In numerical control applications, the use of POD in open loop control of fluids described by Navier Stokes type PDE can be found in [29, 28] while its first use in feedback control design (in the context of smart material structures) is reported in [5]. Other recent applications in feedback control can be found in [1, 2, 24, 23, 25] while POD use in inverse problems for damage detection is first found in [9].

Another type of reduced basis method, the Lagrange model reduction technique, has been numerically studied in [21, 22] (in the context of approximation and control of fluid flows) and in [5, 15] (in approximation and control of thin shell dynamics). This model reduction technique employs the snapshots themselves as basis functions. As detailed in [5, 15], the method possesses inherent difficulties since the user must rely on knowledge of the solution of the system in order to obtain linearly independent snapshots. The question of which parameter values (or time instances in the case vibrating structures) to use for the snapshots in order to capture the key characteristics of the system is another difficult issue to be addressed in the Lagrange reduced basis method. These questions, as we shall see in Section 3.2, are of little concern in the POD approach.

In this paper, we employ the POD model reduction technique in real-time experimental control of a beam structure. The simplicity of the beam structure (i.e., the relatively low dimension of the resulting system in the Galerkin expansion using full order basis functions such as cubic splines) allows us to implement real-time *full order* based control and compare these results with control based on the POD *reduced order* method. In Section 2, the governing equations are presented and existing theories regarding well-posedness of the model are summarized. Approximation methods regarding the *full order method* and *POD reduced order method* are presented in Section 3. Control methodologies are given in Section 4 and experimental results can be found in Section 5. Finally, we offer some concluding remarks in Section 6 relating our POD based methods to standard finite element and modal based control techniques.

2 Beam Model

In this section, we briefly present the equations governing transverse displacements of an Euler-Bernoulli beam with Kelvin-Voigt damping and cantilevered boundary conditions. We also summarize existing results regarding well-posedness of the model. We denote the beam length, width, thickness, density, Young's modulus and Kelvin-Voigt damping by

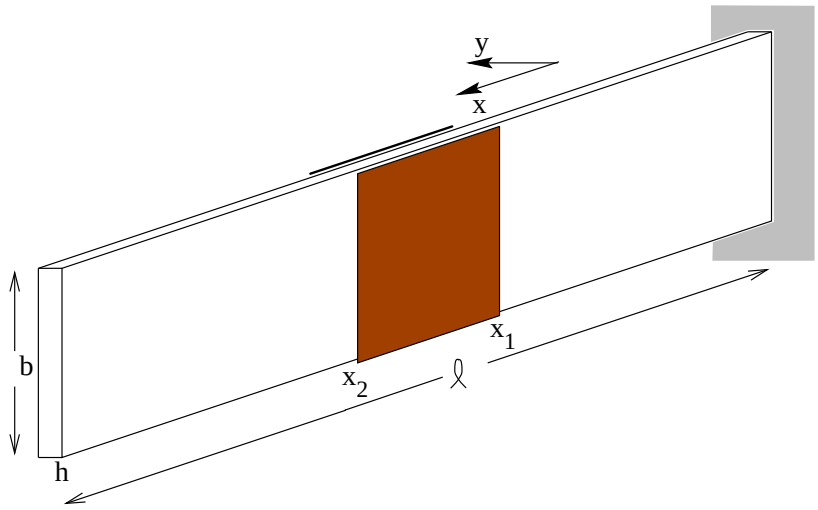

Figure 1: Cantilever beam with piezoceramic patches

ℓ, b, h, ρ, E and c_D, respectively. The origin is taken to be at the clamped edge of the beam, and the axial direction is denoted by the x-axis (see Figure 1). A pair of identical piezoceramic patches are bonded on opposite sides of the beam with edges located at x_1 and x_2. Passive patch contributions arising from material changes due to the presence of the patches are included in the model. Patch parameters are denoted by the subscript pe, thus, the patch thickness, width, density, Young's modulus and Kelvin-Voigt damping are given by $h_{pe}, b_{pe}, \rho_{pe}, E_{pe}$ and c_{Dpe}, respectively. We denote the piezoelectric constant relating mechanical strain and applied electric field by d_{31}. Finally, we denote the transverse displacement by y and the voltages applied to the front and back patches by V_1 and V_2, respectively.

As derived in [11], the transverse (or bending) equation of the beam is given in terms of resultant moments bM_x by

$$\tilde{\rho}\frac{\partial^2 y}{\partial t^2} - \frac{\partial^2 (bM_x)}{\partial x^2} + \frac{\partial^2 (bM_x)_{pe}}{\partial x^2} = f \ . \tag{1}$$

Passive patch contributions are incorporated in the model above and hence the linear mass density $\tilde{\rho}(x) = \rho hb + 2b\rho_{pe}h_{pe}\chi_{pe}(x)$ is piecewise constant. The characteristic function $\chi_{pe}(x)$ employed to isolate patch contributions is defined by

$$\chi_{pe}(x) = \begin{cases} 1 & , \quad x_1 \le x \le x_2 \\ 0 & , \quad \text{otherwise} \ . \end{cases} \tag{2}$$

Incorporating both internal damping and material changes due to the presence of the patches, the internal moment resultant bM_x has the form

$$bM_x(t,x) = -\widetilde{EI}(x)\frac{\partial^2}{\partial x^2}y(t,x) - \widetilde{c_D I}(x)\frac{\partial^3}{\partial x^2 \partial t}y(t,x) \ , \tag{3}$$

where

$$\widetilde{EI}(x) = E\frac{h^3 b}{12} + \frac{2b}{3}E_{pe}a_3\chi_{pe}(x) \quad , \qquad \widetilde{c_D I}(x) = c_D\frac{h^3 b}{12} + \frac{2b}{3}c_{Dpe}a_3\chi_{pe}(x) \ , \tag{4}$$

and $a_3 = (h/2 + h_{pe})^3 - h^3/8$ (we refer the reader to [11, Chapter 3] for details regarding patch contributions to the internal moment resultant). When voltages are applied to the front and back patches, the induced external moment $(bM_x)_{pe}$ is given by

$$(bM_x)_{pe}(t,x) = \frac{1}{2}E_{pe}bd_{31}(h + h_{pe})\chi_{pe}(x)[V_1(t) - V_2(t)] \ . \tag{5}$$

External transverse forces acting on the beam are modeled by the function $f(t,x)$. Cantilever boundary conditions are given by

$$y(t,0) = \frac{\partial y}{\partial x}(t,0) = 0, \qquad M_x(t,\ell) = \frac{\partial}{\partial x}M_x(t,\ell) = 0 \ , \tag{6}$$

and initial conditions are denoted by

$$y(0,x) = y_0(x), \qquad \frac{\partial y}{\partial t}(0,x) = y_1(x) \ . \tag{7}$$

To reduce regularity requirements in the discontinuous moment resultants we employ the weak formulation of (1) given by

$$\begin{aligned}
&\int_0^\ell \rho h b\frac{\partial^2 y(t,x)}{\partial t^2}\phi(x)dx + \int_{x_1}^{x_2} 2b\rho_{pe}h_{pe}\frac{\partial^2 y(t,x)}{\partial t^2}\phi(x)dx \\
&+ \int_0^\ell EI\frac{\partial^2 y(t,x)}{\partial x^2}\frac{\partial^2\phi(x)}{\partial x^2}dx + \int_{x_1}^{x_2}\frac{2b}{3}E_{pe}a_3\frac{\partial^2 y(t,x)}{\partial x^2}\frac{\partial^2\phi(x)}{\partial x^2}dx \\
&+ \int_0^\ell c_D I\frac{\partial^3 y(t,x)}{\partial x^2\partial t}\frac{\partial^2\phi(x)}{\partial x^2}dx + \int_{x_1}^{x_2}\frac{2b}{3}c_{Dpe}a_3\frac{\partial^3 y(t,x)}{\partial x^2\partial t}\frac{\partial^2\phi(x)}{\partial x^2}dx \\
&= \int_{x_1}^{x_2}\frac{1}{2}E_{pe}bd_{31}(h + h_{pe})\Big(V_1(t) - V_2(t)\Big)\frac{\partial^2\phi(x)}{\partial x^2}dx \\
&\quad + \int_0^\ell f(t,x)\phi(x)dx \ ,
\end{aligned} \tag{8}$$

for all $\phi(x) \in V = H_L^2(0,\ell) = \{\phi \in H^2(0,\ell) | \phi(0) = \phi'(0) = 0\}$. Here $I = bh^3/12$, the state space is taken to be the Hilbert space $H = L^2(0,\ell)$, and we seek solutions $y(t,\cdot) \in V$.

Using a variational framework, the existence and uniqueness of the solution to (8) has been established in [11, Chapter 4] and those results will be summarized here. We reformulate (8) in a variational setting by first defining the sesquilinear forms σ_1 and σ_2 defined on $V \times V \to \mathbb{C}$ by

$$\sigma_1(\phi,\psi) = \left\langle \widetilde{EI}\phi'', \psi'' \right\rangle \quad \text{and} \quad \sigma_2(\phi,\psi) = \left\langle \widetilde{c_D I}\phi'', \psi'' \right\rangle \tag{9}$$

for all $\phi, \psi \in V$. Note that V and H form a Gelfand triple $V \hookrightarrow H \simeq H^* \hookrightarrow V^*$, i.e., V is continuously and densely embedded in H and we identify H^* with H through the Riesz map (see [42, pages 165,261]). We take the duality pairing $\langle \cdot, \cdot \rangle_{V^*,V}$ to be the extension by continuity of the inner product $\langle \cdot, \cdot \rangle_H$ from $V \times H$ to $V^* \times H$. We then define $(bM_x)_{pe} + f \in V^*$ by $((bM_x)_{pe} + f)(\phi) = \langle (bM_x)_{pe}(t), \phi'' \rangle + \langle f(t), \phi \rangle$ for $\phi \in V$. Equation (8) can now be abstractly formulated as

$$\langle \tilde{\rho} \ddot{y}(t), \phi \rangle_{V^*,V} + \sigma_2(\dot{y}(t), \phi) + \sigma_1(y(t), \phi) = \langle (bM_x)_{pe}(t) + f(t), \phi \rangle_{V^*,V} \ . \tag{10}$$

It can be readily verified that (i) the stiffness sesquilinear form σ_1 is symmetric, V-continuous and V-elliptic, and (ii) the damping sesquilinear form σ_2 is V-continuous and V-elliptic. Under the additional assumptions (iii) the forcing terms $(bM_x)_{pe} + f$ satisfy the regularity condition $(bM_x)_{pe} + f \in L^2((0,T), V^*)$, (iv) $y_0 \in V$ and (v) $y_1 \in H$ then Theorem 4.1 in [11] (which is first proven in [8]) states that there exists a unique solution y of (10) with the regularity properties $y \in L^2((0,T), V), \dot{y} \in L^2((0,T), V)$ and $\ddot{y} \in L^2((0,T), V^*)$. Moreover, the solutions depend continuously on the data $(y_0, y_1, (bM_x)_{pe} + f)$ in that the map $(y_0, y_1, (bM_x)_{pe} + f) \to (y, \dot{y})$ is continuous from $V \times H \times L^2((0,T), V^*)$ to $L^2((0,T), V) \times L^2((0,T), V)$.

For control applications, the equivalent operator formulation of the abstract variational form (10) is more familiar. Again we give a brief summary of the theoretical results. Under the assumption that σ_1 and σ_2 are V-continuous, we can define the operators $\mathcal{A}_1, \mathcal{A}_2$ from $V \to V^*$ given by

$$(\mathcal{A}_1 \psi)(\phi) = \sigma_1(\phi, \psi) \ , \qquad (\mathcal{A}_2 \psi)(\phi) = \sigma_2(\phi, \psi) \ , \tag{11}$$

for all $\phi, \psi \in V$. Then an equivalent formulation of equation (10) is given by

$$\tilde{\rho} \ddot{y}(t) + \mathcal{A}_1 y(t) + \mathcal{A}_2 \dot{y}(t) = (bM_x)_{pe}(t) + f(t) \qquad \text{in } V^* \ . \tag{12}$$

The first order formulation of (12) is obtained by first defining the product spaces $\mathcal{V} = V \times V$ and $\mathcal{H} = V \times H$. We then let

$$\mathcal{F}(t) = \begin{bmatrix} 0 \\ f(t) \end{bmatrix} \quad , \quad \mathcal{B} = \frac{1}{2} E_{pe} b d_{31} (h + h_{pe}) \begin{bmatrix} 0 & 0 \\ \chi_{pe}(x) & -\chi_{pe}(x) \end{bmatrix} , \tag{13}$$

and $u(t) = [V_1(t), V_2(t)]^T$. Finally we define the system operator $\mathcal{A}$ in matrix form by

$$\begin{aligned} \mathcal{A} &= \begin{bmatrix} 0 & I \\ -\mathcal{A}_1 & -\mathcal{A}_2 \end{bmatrix} \\ \text{dom}\mathcal{A} &= \{ \chi = (\phi, \psi) \in \mathcal{H} | \psi \in V \text{ and } \mathcal{A}_1 \phi + \mathcal{A}_2 \psi \in H \} \end{aligned} \tag{14}$$

and the strong first order form of (12) is now given by

$$\begin{aligned} \dot{w}(t) &= \mathcal{A} w(t) + \mathcal{B} u(t) + \mathcal{F}(t) \\ w(0) &= w_0 = (y_0, y_1) \ , \end{aligned} \tag{15}$$

where $w = (y, \dot{y})$. The mild solution to (15) is given by

$$w(t) = \mathcal{T}(t)w_0 + \int_0^t \mathcal{T}(t-s)[\mathcal{B}u(s) + \mathcal{F}(s)]ds \tag{16}$$

and its existence, uniqueness and equivalence to the variational solution is detailed in [11]. Here $\mathcal{T}$ is the semigroup generated by $\mathcal{A}$ (see [34] for details regarding semigroup generators).

3 Galerkin Discretization and Model Reduction

A Galerkin method employing cubic splines as basis functions was used to discretize the system (8). As discussed in [16], cubic splines were chosen over modes since for the system under consideration, explicit expressions of the modes and natural frequencies are not readily available. In order to use mode shapes in the expansion, they must first be numerically approximated or experimentally determined. Moreover, the piecewise discontinuities in the density, stiffness and damping coefficients arising due to contributions by the piezoceramic patches cause difficulties for the use of standard finite element packages since the meshes must be aligned with the regions bounded by the patches. Moreover, finite-difference approximations are not employed due to difficulties associated with high-order equations in the beam model.

The standard Galerkin approximation employing cubic splines is efficient for numerical simulations but the size of the resulting finite dimensional system is still not suitable for *real-time* feedback control implementation. Hence we investigate the use of Proper Orthogonal Decomposition reduced basis methods in decreasing the dimension of the approximating system.

In Section 3.1, we briefly discuss the Galerkin discretization method, and specify the cubic spline basis functions employed. We denote the use of modified cubic spline basis functions in the discretization by *full order methods*. In Section 3.2, the ideas underlying the Proper Orthogonal Decomposition reduced basis method are presented. This method is referred to as the *reduced basis method*. Finally, in Section 3.3, we report in detail the methods and discretization sizes employed in numerically implementing the methods presented in this section.

3.1 Galerkin Approximation

The approximate solution $y \in L^2((0,T),V)$ to (8) is obtained by replacing the space V with appropriate finite dimensional subsets $V^{\mathcal{N}} = \text{span}\{\mathcal{B}_i\}_{i=1}^{\mathcal{N}} \subset H = L^2(0,\ell)$ and performing the Galerkin expansion

$$y^{\mathcal{N}}(t,x) = \sum_{i=1}^{\mathcal{N}} z_i(t)\mathcal{B}_i(x) \ . \tag{17}$$

The approximating finite dimensional subsets $V^{\mathcal{N}}$ are chosen to satisfy the condition

(H1) for any $\phi \in V$, there exists a sequence $\left\{\phi^{\mathcal{N}}\right\}_{\mathcal{N}=1}^{\infty}$ in $V^{\mathcal{N}}$ such that $\left\|\phi^{\mathcal{N}} - \phi\right\|_V \to 0$ as $\mathcal{N} \to \infty$.

We then restrict the weak form (8) to $V^{\mathcal{N}}$ with basis functions also used as test functions and $\mathcal{N}$ fixed. (All of the resulting matrices are understood to depend on $\mathcal{N}$ throughout, but for convenience we shall suppress this in our notation.) This yields the matrix system approximating (8) given by

$$\begin{aligned} &(M + M_{pe})\,\ddot{z}(t) + (D + D_{pe})\,\dot{z}(t) + (KE + KE_{pe})\,z(t) = \tilde{F}(t) + \tilde{B}u(t) \\ &z(0) = z_0, \qquad \dot{z}(0) = z_1\ , \end{aligned} \tag{18}$$

where $z(t) = [z_1(t), \ldots, z_{\mathcal{N}}(t)]^T$ is the vector of coefficients. The matrices in (18) are defined by

$$\begin{aligned} &[M]_{k,l} = \rho h b \int_0^\ell \mathcal{B}_l(x)\mathcal{B}_k(x)dx \quad , \quad [M_{pe}]_{k,l} = 2b\rho_{pe}h_{pe}\int_{x_1}^{x_2} \mathcal{B}_l(x)\mathcal{B}_k(x)dx \\ &[KE]_{k,l} = EI \int_0^\ell \mathcal{B}_l''(x)\mathcal{B}_k''(x)dx \quad , \quad [KE_{pe}]_{k,l} = \frac{2b}{3}E_{pe}a_3\int_{x_1}^{x_2} \mathcal{B}_l''(x)\mathcal{B}_k''(x)dx \\ &[D]_{k,l} = c_D I \int_0^\ell \mathcal{B}_l''(x)\mathcal{B}_k''(x)dx \quad , \quad [D_{pe}]_{k,l} = \frac{2b}{3}c_{D_{pe}}a_3\int_{x_1}^{x_2} \mathcal{B}_l''(x)\mathcal{B}_k''(x)dx \\ &[\tilde{F}]_k(t) = \int_0^\ell f(x,t)\mathcal{B}_k(x)dx \quad , \quad [\tilde{\mathcal{B}}]_{k,1} = \tfrac{1}{2}E_{pe}bd_{31}(h+h_{pe})\int_{x_1}^{x_2} \mathcal{B}_k''(x)dx \\ &u(t) = [V_1(t)\ ,\ V_2(t)]^T \quad , \quad [\tilde{\mathcal{B}}]_{k,2} = -\tfrac{1}{2}E_{pe}bd_{31}(h+h_{pe})\int_{x_1}^{x_2} \mathcal{B}_k''(x)dx\ . \end{aligned} \tag{19}$$

The first order reformulation of (18),

$$\begin{aligned} &\dot{w}(t) = Aw(t) + Bu(t) + F(t) \\ &w(0) = w_0 = [z_0, z_1]^T\ , \end{aligned} \tag{20}$$

is obtained by letting $w = (z, \dot{z})^T$,

$$A = \begin{bmatrix} I & 0 \\ 0 & M + M_{pe} \end{bmatrix}^{-1} \begin{bmatrix} 0 & I \\ -(KE + KE_{pe}) & -(D + D_{pe}) \end{bmatrix}\ , \tag{21}$$

$$F(t) = \begin{bmatrix} I & 0 \\ 0 & M + M_{pe} \end{bmatrix}^{-1} \begin{bmatrix} 0 \\ \tilde{F}(t) \end{bmatrix}\ , \text{ and } \quad B = \begin{bmatrix} I & 0 \\ 0 & M + M_{pe} \end{bmatrix}^{-1} \begin{bmatrix} 0 \\ \tilde{B} \end{bmatrix}\ . \tag{22}$$

Cubic splines were employed as basis functions in the standard (or full order) Galerkin expansion. This choice of basis functions was motivated by smoothness requirements, accuracy, adaptability to different boundary conditions and flexibility with regard to internal and external patch contributions. To define the *standard* cubic splines, we first partition

the interval $[0,\ell]$ with grid points $x_n = nh_x, h_x = \ell/N,\ n = 0,\ldots,N$. The standard cubic splines are then defined by

$$b_n(x) = \frac{1}{h_x^3}\begin{cases} (x-x_{n-2})^3, & x \in [x_{n-2}, x_{n-1}] \\ h_x^3 + 3h_x^2(x-x_{n-1}) + 3h_x(x-x_{n-1})^2 - 3(x-x_{n-2})^3, & x \in [x_{n-1}, x_n] \\ h_x^3 + 3h_x^2(x_{n+1}-x) + 3h_x(x_{n+1}-x)^2 - 3(x_{n+1}-x)^3, & x \in [x_n, x_{n+1}] \\ (x_{n+2}-x)^3, & x \in [x_{n+1}, x_{n+2}] \\ 0, & \text{otherwise}\ , \end{cases} \tag{23}$$

for $n = -1,\ldots,N+1$,(see [36]). These standard splines must be modified to satisfy the clamped edge boundary conditions (6). The *modified* cubic splines satisfying the zero slope and zero displacements conditions at $x = 0$ are given by

$$\mathcal{B}_n(x) = \begin{cases} b_0(x) - 2b_{-1}(x) - 2b_1(x) & ,\ n = 1 \\ b_n(x) & ,\ n = 2,\cdots,N+1 \quad , \end{cases} \tag{24}$$

for a total of $N+1$ basis functions. These basis elements satisfy

$$\mathcal{B}_n(0) = \mathcal{B}_n'(0) = 0 \quad n = 1,\cdots,N+1\ .$$

Therefore, if N standard cubic splines are employed, the system (20) is of dimension $\mathcal{N} = 2(N+1)$ (note that the factor 2 comes from reformulating the system in first order form).

A general framework for the convergence of full order solutions has been given in the electronic version of [7]. Under the assumption that (H1) is satisfied by the cubic splines, Lemma 4.1 in [7] guarantees convergence of the full order solution to the infinite dimensional solution of (8).

3.2 Basis Reduction via Proper Orthogonal Decomposition

The POD *reduced order basis method* we discuss here involves the use of a smaller approximating subspace of $V^{\mathcal{N}}$. To differentiate full order basis functions from reduced basis elements, we denote the i^{th} full order basis functions by $\mathcal{B}_i$ while we denote the i^{th} POD reduced basis function by Φ_i. We also denote the full order dimension index by $\mathcal{N}$ and reduced order dimension index by $\mathcal{N}_P$.

To create the POD basis elements, we take N_s temporal snapshots of the model, $\{y^{\mathcal{N}}(t_j,x)\}_{j=1}^{N_s}$, and seek basis elements of the form

$$\Phi_i(x) = \sum_{j=1}^{N_s} \alpha_j^i y^{\mathcal{N}}(t_j,x)\ . \tag{25}$$

The snapshots can either be numerical solutions or physical measurements of the state. We require each basis element Φ_i to resemble all the snapshots in the sense that it maximizes

$$\frac{1}{N_s}\sum_{j=1}^{N_s} \left|\left\langle y^{\mathcal{N}}(t_j,\cdot), \Phi_i(\cdot)\right\rangle\right| \quad , \quad \text{subject to } \langle \Phi_i, \Phi_i\rangle = \|\Phi_i\|^2 = 1\ . \tag{26}$$

As detailed in [5, 12, 15, 29], the coefficients of the i^{th} POD basis function (i.e., the α_j^i in (25)) are the elements of the i^{th} eigenvector of the covariance matrix C, where C is defined by

$$[C]_{k,\ell} = \frac{1}{N_s} \left\langle y^{\mathcal{N}}(t_k, \cdot), y^{\mathcal{N}}(t_\ell, \cdot) \right\rangle \ , \quad k, \ell = 1, \ldots, N_s \ . \tag{27}$$

Since C is Hermitian and nonnegative, we can order the eigenvalues $\lambda_1 \geq \lambda_2 \geq \ldots \geq \lambda_{N_s} \geq 0$ and it has a complete set of orthogonal vectors. Note that the eigenvectors are normalized in such a way that

$$\alpha^k \cdot \alpha^\ell = \begin{cases} 0, & k \neq \ell \\ \dfrac{1}{N_s \lambda_k}, & k = \ell \ . \end{cases}$$

The POD basis functions Φ_i were shown to be orthonormal in [29]. It was also shown in [12] that the numerical solution using the POD basis functions in the expansion is optimal in the sense that it maximizes the time average of the displacements. This optimality of the POD basis functions is summarized in [12, Prop. 2.3].

Lemma 1 *Let $\{\Phi_1, \Phi_2, \ldots, \Phi_{N_s}\}$ denote the orthonormal set of POD basis elements and $\lambda_1 \geq \ldots \geq \lambda_{N_s}$ denote the corresponding set of eigenvalues. If $y^{N_s} = \sum_{i=1}^{N_s} b_i(t)\Phi_i$ denotes the approximation to y with respect to this basis, then for any arbitrary orthonormal basis $\{\psi_1, \psi_2, \ldots, \psi_{N_s}\}$, the following hold*

1. $\ll b_i(t) b_j^*(t) \gg \ = \ \lambda_i \delta_{ij}$, *where $\ll \cdot \gg$ denotes the average over time,*

2. *for every N_s,* $\displaystyle\sum_{i=1}^{N_s} \ll b_i(t) b_i^*(t) \gg \ = \sum_{i=1}^{N_s} \lambda_i \geq \sum_{i=1}^{N_s} \ll a_i(t) a_i^*(t) \gg \ ,$

where the $a_i(t)$ are coefficients of the approximation to y, $y_\psi^N = \sum_{i=1}^{N_s} a_i(t)\psi_i$, using the arbitrary orthonormal basis $\{\psi_j\}_{j=1}^{N_s}$.

Lemma 1 provides a systematic way of creating an $\mathcal{N}_P$ dimensional POD reduced basis (where $\mathcal{N}_P \ll N_s$) out of N_s snapshots. Since the most significant POD modes correspond to the largest eigenvalues, we take $\mathcal{N}_P$ to be the smallest integer such that $\sum_{i=1}^{\mathcal{N}_P} \lambda_i \simeq \sum_{i=1}^{N_s} \lambda_i$. The ratio gives the percentage of the mean square error when the first $\mathcal{N}_P$ POD modes are eliminated in the reduced basis representation (see [24] for details and the references cited therein). Initial approximation results for the use of POD elements in Galerkin schemes are given in [26].

As emphasized in [5], we note that for the POD reduced basis method, a fundamental practical question is not of convergence but of *(i) how to take an ensemble of snapshots which lead to a good approximation of the full order solution* and *(ii) how to choose a reduced set of basis elements that will capture the approximation properties of the original ensemble.* It is difficult to address the first question since it requires knowledge of the solution of the original physical system. Since the POD reduced basis method does not use the snapshots as basis themselves, the question of independence of snapshots is not

important. Hence one way to capture the characteristics of the full order solution is to take a sufficiently large number of snapshots. This is an acceptable strategy since the covariant matrix C and the POD basis functions are computed offline. In relation to the second question, Lemma 1 provides a systematic method to choose a reduced set of basis elements out of the N_s snapshots. The lemma shows how well the first $\mathcal{N}_P$ POD basis functions approximate the displacement average contained in all the snapshots (see [5]).

3.3 Numerical Implementation

Numerical discretization using the full order method was performed using 16 standard cubic splines, resulting in an $\mathcal{N} = 34$ dimensional matrix system (20). Integration of the basis functions (see (19)) were performed using a four point Gaussian quadrature rule with $N_q = 64$ nodes. This quadrature is of the form

$$\int_0^{\ell} f(x)dx \approx \sum_{l=1}^{N_q} \sum_{k=1}^{4} c_k f(x_{kl}) \ , \tag{28}$$

where the quadrature weights c_k and points x_{kl} on the l^{th} interval $[l-1, l] * h_q, hq = \ell/N_q$ are given by

$$\begin{aligned}
c_1 &= \frac{49}{6(18+\sqrt{30})} \cdot \frac{h_q}{2} \quad , \quad x_{1l} = h_q \left[\frac{1}{2} - \frac{\sqrt{15+2\sqrt{30}}}{2\sqrt{35}} \right] \\
c_2 &= \frac{49}{6(18-\sqrt{30})} \cdot \frac{h_q}{2} \quad , \quad x_{2l} = h_q \left[\frac{1}{2} - \frac{\sqrt{15-2\sqrt{30}}}{2\sqrt{35}} \right] \\
c_3 &= \frac{49}{6(18-\sqrt{30})} \cdot \frac{h_q}{2} \quad , \quad x_{3l} = h_q \left[\frac{1}{2} + \frac{\sqrt{15-2\sqrt{30}}}{2\sqrt{35}} \right] \\
c_4 &= \frac{49}{6(18+\sqrt{30})} \cdot \frac{h_q}{2} \quad , \quad x_{4l} = h_q \left[\frac{1}{2} + \frac{\sqrt{15+2\sqrt{30}}}{2\sqrt{35}} \right] \ ,
\end{aligned}$$

(see [40] for details).

To obtain the snapshots for creating the POD basis elements, the uncontrolled full order system excited by a voltage spike to the back patch was numerically simulated on the interval $t = 0$ to $t = 0.5$ seconds. The voltage spike is triangular in shape with a duration of 0.001 s and a magnitude at the peak of 90 V. A variable stepsize stiff ODE solver was employed in time stepping the system. One hundred evenly spaced time snapshots ($N_s = 100$) were taken from which the 100×100 covariant matrix C given by (27) was created. After obtaining the eigenvectors and eigenvalues of the covariant matrix, the number of POD basis functions was determined by ensuring the percentage of the displacement average of all snapshots contained by the reduced basis was at least 90%. It can be seen in Table 1 that this requirement is satisfied even with 1 POD basis function.

$\mathcal{N}_P$	1	2	3	4	5	6
$\sum_{i=1}^{\mathcal{N}_P} \lambda_i / \sum_{i=1}^{N_s} \lambda_i$	.9008399	.9999942	.9999988	.9999996	1.0	1.0

Table 1: Ratio of full order model snapshots captured by the POD basis functions; $N_s = 100$ snapshots; $\mathcal{N}_P$ is the number of POD reduced basis elements.

4 LQG Compensator Control

Infinite dimensional control for the system (15) where $\mathcal{F} \equiv 0$ or $\mathcal{F}$ is periodic has been studied extensively in [7, 11, 37]. Since our goal is to implement real time control, we will concentrate on finite dimensional control methods for the matrix equation (20) and consider only transient shell vibrations ($F \equiv 0$). This case we consider is suitable when controlling vibrations caused by an impulse force (such as a hammer impact), or when the structure responds to a perturbation and vibrates to a steady state.

A state *estimator* must be employed in the control scheme due to the nature of the sensing device employed in the experiment. Vibrations measured at only one point $\hat{x}$ on the beam by the proximity probe are used as observations. Thus, we consider observations of the state given by the operator $\mathcal{C} : V \to Y, w_{ob} = \mathcal{C}w(t)$, where Y is the observation space and $w_{ob}(t) = y^{\mathcal{N}}(t, \hat{x}) \approx y(t, \hat{x})$.

We present the approximate LQG control problem with no exogenous input in Section 4.1. In order to experimentally implement the control method in Section 4.1, we must modify the assumptions that observations can be obtained at *any* time throughout the time interval of interest, and that the state and state estimator can be exactly integrated. Thus, we discuss the discrete-time compensator problem in Section 4.2.

4.1 Continuous-time Finite Dimensional Control

The infinite horizon control problem is

$$\text{minimize} \quad J(u, w_0) = \int_0^\infty \{\langle Qw(t), w(t)\rangle + \langle Ru(t), u(t)\rangle\} dt \tag{29}$$

subject to the matrix equation

$$\begin{aligned} \dot{w}(t) &= Aw(t) + Bu(t) \ , \quad w(0) = w_0 \\ w_{ob}(t) &= Cw(t) \ . \end{aligned} \tag{30}$$

Here C is the observation matrix which maps $w(t)$ with the observation $w_{ob}(t)$, while Q and R are control parameter matrices used to weigh the state and control, respectively. We follow the control methods numerically implemented in [5, 18] where the optimal control is given by

$$u(t) = -Kw_c(t) \ . \tag{31}$$

Here the state estimator is given by

$$\begin{aligned} \dot{w}_c(t) &= Aw_c(t) + Bu(t) + F[w_{ob}(t) - Cw_c(t)] \\ w_c(0) &= w_{c_0} = Cw_0 \ , \end{aligned} \tag{32}$$

(see [11] for details) and the optimal feedback gain (regulator) K and observer (Kalman filter) gain F are given by

$$\begin{aligned} K &= R^{-1}B^T\Pi \\ F &= \hat{\Pi}C^T\hat{R}^{-1} \ , \end{aligned} \tag{33}$$

where Π and $\hat{\Pi}$ are solutions to the algebraic Riccati equations

$$\begin{aligned} \Pi A + A^T\Pi - \Pi BR^{-1}B^T\Pi + Q = 0 \\ \hat{\Pi}A^T + A\hat{\Pi} - \hat{\Pi}C^T\hat{R}^{-1}C\hat{\Pi} + \hat{Q} = 0 \ , \end{aligned} \tag{34}$$

respectively. Playing a similar role to that of Q and R in the control problem, the matrices $\hat{Q}$ and $\hat{R}$ are design criteria for the state estimator.

The structure of the observation matrix C depends on the sensor employed in the experiment. In our model, the sensor is a proximity probe located at the back of the beam sensing displacements at the point $\hat{x}$. The observation matrix C is thus of the form

$$C = \left[B_1(\hat{x}), \ldots, B_{\mathcal{N}}(\hat{x}), \underbrace{0, \ldots, 0}_{\mathcal{N}} \right] \ ,$$

where the $B_i(\hat{x})$'s are the basis functions evaluated at $\hat{x}$.

It was shown in [7, 11] (see also [4]) that the approximate controls and Riccati solutions based on *full order* methods converge (as $\mathcal{N} \to \infty$) to the corresponding infinite dimensional optimal control and Riccati operators. The assumptions needed to establish convergence of the full order Riccati operators and optimal controls are that (i) (H1) holds, (ii) V is compactly embedded in H, and (iii) the infinite and finite dimensional systems are stabilizable and detectable. For the POD based controls, the questions of convergence are not meaningful. The issue, rather, is how the reduced order based controls would perform when implemented in physical infinite dimensional systems. In a previous investigation, the issue was computationally addressed when POD reduced order based controls were applied to the full order system in controlling thin cylindrical shell vibrations (see [5]). In Section 5, we further address the issue of effectiveness on the orginal infinite dimensional system by implementing POD based controls on a physical system.

4.2 Discrete-Time Finite Dimensional Control

In experimental applications, the signals from the sensors are digitized and the real-time processor can only perform at a discrete sample rate Δt. Thus, the state estimator equation (32) can only be evolved in time in discrete time steps, and the control voltage can be only computed at this rate. The numerical ODE approximation method to solve the

state estimator equation must satisfy the following criteria: (i) the control $u(t_j)$ must be calculated before the arrival of the data at the next time step $t_{j+1} = t_j + \Delta t$, (ii) the method must be sufficiently accurate to resolve system dynamics and (iii) since the ode systems are often stiff, the method must be A-stable or α-stable. We chose a modified backward Euler method given in [11, Chapter 8.2.1]. The fast sample rate (and hence small Δt) at which we can carry out the experiment allows the use of this method. An A-stable modified backward Euler method integrating the state estimator (32) at time t_{j+1} is given by

$$\begin{aligned} w_{c_{j+1}} &= (I - \Delta t A_c)^{-1} w_{c_j} + \Delta t (I - \Delta t A_c)^{-1} F w_{ob}(t_j) \\ &= R(A_c) w_{c_j} + \Delta t R(A_c) F w_{ob}(t_j) \ , \end{aligned} \tag{35}$$

where $A_c = A - BK - FC$, $R(A_c) = (I - \Delta t A_c)^{-1}$ and the constant time step is $\Delta t = t_{j+1} - t_j$. Note that the method is modified from standard backward Euler methods since the observation $w_{ob}(t_j)$ at future time steps are not available. We now summarize the discrete-time algorithm in Algorithm 1, which is essentially Algorithm 8.5 in [11]

Offline	(i)	Construct matrices $A, B, C, Q, R, \hat{Q}, \hat{R}$
	(ii)	Solve Riccati equations (34) for Π and $\hat{\Pi}$
	(iii)	Construct $K = R^{-1} B^T \Pi, F = \hat{\Pi} C^T \hat{R}^{-1}$, and $A_c = A - BK - FC$
	(iv)	Construct $R(A_c) = (I - \Delta t A_c)^{-1}$ and $R(A_c)F = (I - \Delta t A_c)^{-1} F$
Online	(i)	Collect observation $w_{ob}(t_j)$
	(ii)	Time step the discrete compensator system $w_{c_{j+1}} = R(A_c) w_{c_j} + \Delta t R(A_c) F w_{ob}(t_j)$
	(iii)	Calculate the voltage $u(t_{j+1}) = -K w_{c_{j+1}}$

Algorithm 1: Discrete compensator for systems running at a sample rate of Δt.

5 Real-Time Feedback Control Implementation

In Table 2, we report the dimensions and parameters of our experimental beam structure depicted in Figure 2. The aluminum beam parameters ρ, E, c_D and the lead zirconate titanate piezoceramic patch parameters $\rho_{pe}, E_{pe}, c_{Dpe}, d_{31}$ were obtained from the manufacturers. Typically, parameter estimation techniques must be carried out in order to obtain more accurate values but since the goal of this investigation is the application of the POD reduced basis method in real time control, we do not consider the inverse problem in detail here. Rather, we refer the reader to [11, Chapter 5.4] for discussions and experimental results regarding estimation of parameters and inverse problems involving the beam.

Beam	Patch
$\ell = 0.286\ m$	$h_{pe} = 5.3 \times 10^{-4}\ m$
$h = 0.001\ m$	$\rho_{pe} = 7.45 \times 10^{3}\ kg/m^3$
$b = 0.2543\ m$	$E_{pe} = 6.4 \times 10^{10}\ N/m^2$
$\rho = 3.438 \times 10^{3}\ kg/m^3$	$c_{Dpe} = 3.96 \times 10^{5}\ Ns/m^2$
$E = 7.062 \times 10^{10}\ N/m^2$	$d_{31} = 262 \times 10^{-12}\ m/V$
$c_D = 1.04 \times 10^{6}\ Ns/m^2$	$x_1 = 0.02041\ m$
$\hat{x} = 0.11076\ m$	$x_2 = 0.04592\ m$

Table 2: Beam and Patch Parameters

Figure 2: Experimental beam with piezoceramic patches

Numerical simulations were performed to obtain reasonable values of the control parameter matrices $Q, R, \hat{Q}$ and $\hat{R}$ to be used in (29) and (34). We sought parameters leading to maximum control voltages within the $\pm 100V$ range of the patches while at the same time providing good attenuation (see [5, 17] for discussions regarding the choice of control parameters in shell control simulations). The matrices employed were of the form

$$\begin{aligned} Q &= d_1 \begin{bmatrix} KE + KE_{pe} & 0 \\ 0 & M + M_{pe} \end{bmatrix} \quad , \quad R = r_1 I^{p\times p}\ , p = 1 \\ \hat{Q} &= \hat{d}_1 \begin{bmatrix} I^N & 0 \\ 0 & I^N \end{bmatrix} \qquad\qquad , \quad \hat{R} = \hat{r}_1 I^{s\times s}\ , s = 1\ , \end{aligned} \tag{36}$$

where p is the number of actuators and s is the number of sensors. In Table 3, we report the values of $d_1, r_1, \hat{d}_1, \hat{r}_1$, for three discretization sizes: full order system, POD system with 2 POD basis functions, and POD system with 1 POD basis function. To illustrate the expected performance of the control, we also report in Table 3 the maximum of the

real parts of the eigenvalues of the matrices $A, A-BK$ and $A-FC$ for each of the three discretization sizes. It can be seen that the maximum real part of the eigenvalues of the closed loop system $A-BK$ was 3 orders of magnitude less than that of the system matrix A, while for the state estimator, $A-FC$ was 2 orders of magnitudes less. To further illustrate the features of the reduced basis method, the controllability matrices of the linear systems arising from the three discretization sizes were analyzed. *Controllability* is a necessary (but not sufficient) condition for a linear system to be driven to zero starting at any initial state. Linear systems described by the matrices A and B in the first order linear system (20) are *controllable* if the $2\mathcal{N}_P \times 2s\mathcal{N}_P$ controllability matrix $\mathcal{C}(A,B) = [B|AB|A^2B|\cdots|A^{2\mathcal{N}_P-1}B]$, where $A \equiv A^{2\mathcal{N}_P}, B \equiv B^{2\mathcal{N}_P}$, has full rank $2\mathcal{N}_P$. For systems with rank $(\mathcal{C}(A,B)) = m \leq 2\mathcal{N}_P$, any initial condition of the state $z^{2\mathcal{N}_P}$ in the m dimensional subspace of $\mathbb{R}^{2\mathcal{N}_P}$ spanned by the columns of $\mathcal{C}(A,B)$ can be driven to zero (see [14]). Generally speaking, the larger the deficit of $\mathcal{C}(A,B)$ from its maximum possible rank, the more difficulty in stabilizing or controlling the linear system (30). The ranks of the controllability matrices for the three discretization systems are reported in the last row of Table 3. It can be seen that the full order linear system is more difficult to stabilize than that of the two POD systems (whose controllability matrices are of full rank).

	Full Order	$\mathcal{N}_P = 2$	$\mathcal{N}_P = 1$
d_1, r_1	$2 \times 10^8, 0.98$	$6 \times 10^{10}, 1 \times 10^{-4}$	$6 \times 10^{10}, 1 \times 10^{-4}$
$\hat{d}_1, \hat{r}_1$	$1 \times 10^3, 1$	$5 \times 10^8, 1 \times 10^{-1}$	$5 \times 10^8, 1 \times 10^{-1}$
$\max(\Re(\text{eig}(A)))$	$-3.107e-2$	$-3.111e-2$	$-3.112e-2$
$\max(\Re(\text{eig}(A-BK)))$	$-1.215e+1$	$-6.625e+1$	$-6.695e+1$
$\max(\Re(\text{eig}(A-FC)))$	$-8.526e+0$	$-3.445e+0$	$-3.433e+0$
$\frac{\text{rank}(\mathcal{C}(A,B))}{\text{max possible rank}}$	9/34	4/4	2/2

Table 3: Control Parameter Values and some properties of the resulting linear systems due to the three discretization sizes: full order, POD system with 2 basis functions and POD system with 1 basis function.

In Figure 3, we present a diagram of the experimental setup and implementation of the online component of Algorithm 1. Voltage spikes to the back patch (to excite the beam) were generated by a DS1103 dSpace control system. The excitation signal was low pass filtered and amplified before being applied to the back patch. The voltage spike was amplified so as to produce 90 volts at the peak. A proximity probe located at the back of the beam at $x = \hat{x} = 0.11076\ m$ was used to measure displacements and the observation readings were digitized through one analog to digital channel of the dSpace hardware. This observation signal enters the online component of Algorithm 1 as $w_{ob}(t_j)$. By employing the discrete modified backward Euler method (35), the state estimator $w_c(t_{j+1})$ was obtained and multipled with the gain matrix K to produce the control voltage. The control signal was then low pass filtered and amplified before being sent to the front patch. A constant discrete time rate of $\Delta t = 10^{-4}\ s$ was employed in running the real-time processor.

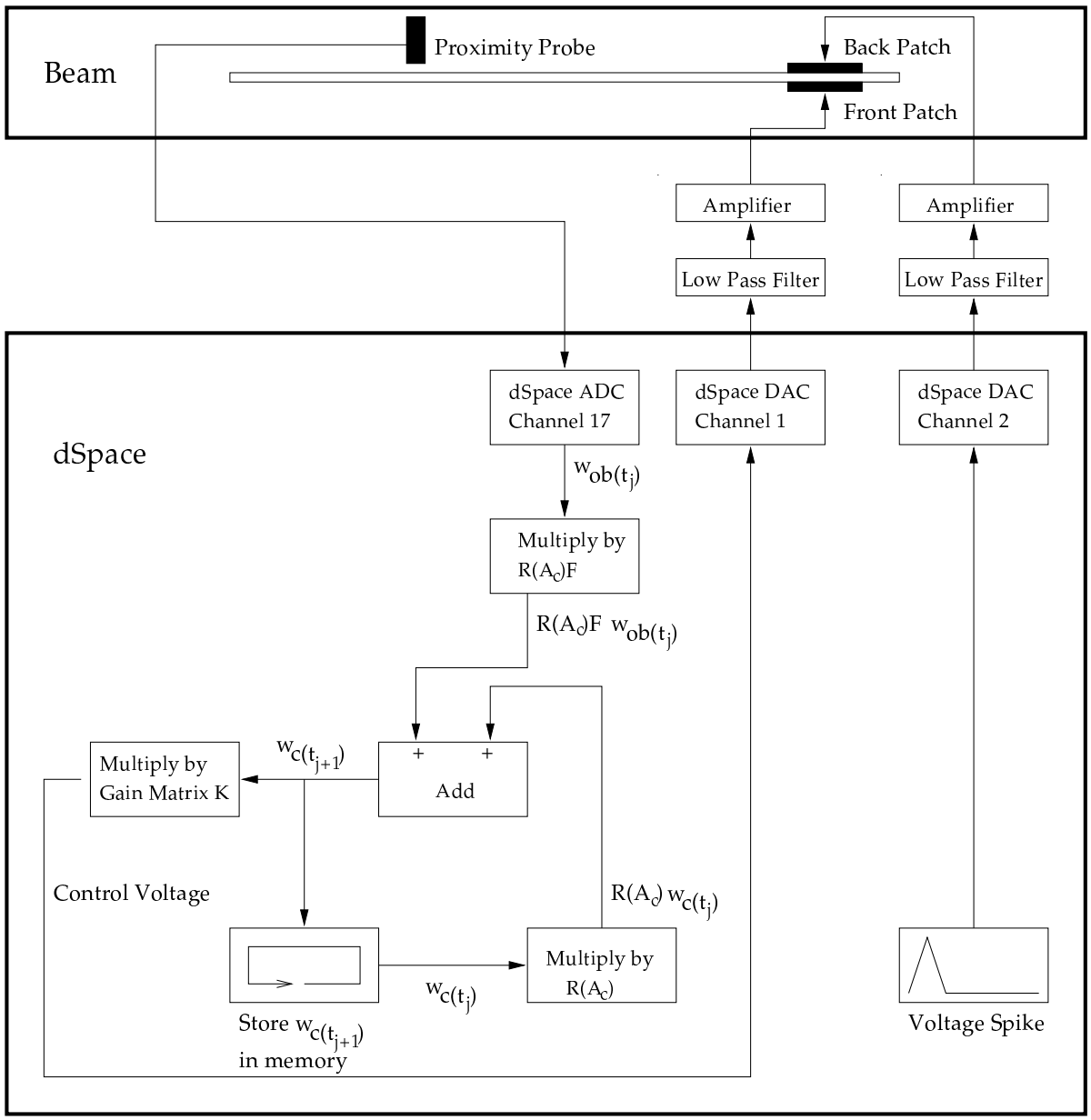

Figure 3: Experimental setup and implementation of online component of Algorithm 1.

In Figure 4, we report the uncontrolled and controlled displacements in the left column and the control voltages in the right column for the three discretization sizes: full order method, POD based control with 2 POD basis elements and POD based control with 1 POD basis element. Note that the three control systems have basically attenuated the displacements after 1 second.

6 Concluding Remarks

Our initial experimental results suggest that application of POD based control in real time control is most promising. Creation of the POD reduced basis using numerical solutions as snapshots is relatively easy to implement since a lot of effort has been invested in developing accurate models and efficient numerical approximation methods for smart material structures. The online component control method (shown in Algorithm 1) can be efficiently implemented in real-time due to the simplicity of the algorithm and the simple programming of the real-time control implementation system employed.

A comparison of the attenuation levels due to three discretization sizes, i.e., full order (34 dimensional linear system), POD with 2 basis functions (4 dimesions) and POD with 1 basis function (2 dimensions) illustrates the feasibility of POD based control in physical implementation. Aside from decreasing the dimension of the linear approximating system, the POD model reduction also results in linear systems that are controllable and observable.

For the particular physical system (a cantilevered beam) used here to illustrate the effectiveness of POD based control methods, one might expect that an effective low order model (dimension ≤ 3) would suffice based on the research literature on modal based methods in structures. However, this does not lessen the importance of our contributions here. First, we note that the POD based methods offer an attractive implementable alternative to modal methods since analytical modes for even the simple piezo mounted beam are not attainable. Moreover, such systems do *not* have normal modes [10], further complicating any modal based computational control method. Furthermore, the computation of POD basis elements is even simpler than computation of modal elements. When compared to standard finite element approaches, the POD based methods offer control authority with much smaller approximating systems and hence are clearly preferable for implementation. In addition, for more complicated structural problems such as those arising in many applications, the POD based methods will offer a far superior approach in implementation of control and stabilization design. Finally, for control design in fluid or electromagnetic systems where modes are difficult if not impossible to find and where finite element approximations result in really large ($\mathcal{N}$ on the order of 10,000-100,000) approximating systems, POD based methods offer even more exciting possibilities

References

[1] J. A. Atwell and B. King, *Proper orthogonal decomposition for reduced basis feedback controllers for parabolic equations*, ICAM Rep. 99-01-01, VPISU, Blackburg, VA, January, 1999; Mathematical and Computer Modeling, to appear.

[2] ——, *Reduced order controllers for spatially distributed systems via proper orthogonal decomposition*, ICAM Rep. 99-07-01, VPISU, Blackburg, VA, July, 1999.

[3] N. Aubry, P. Holmes, J. Lumley, and E. Stone, *The dynamics of coherent structures in the wall region of a turbulent boundary layer*, Journal of Fluid Mechanics, 192 (1988), pp. 115–173.

[4] H. T. Banks and R. C. H. del Rosario, *Convergence of approximations in feedback control of structures*, CRSC TR98-40, North Carolina State University, Raleigh, NC, November, 1998; Mathematical and Computer Modeling, to appear.

[5] H. T. Banks, R. C. H. del Rosario, and R. C. Smith, *Reduced order model feedback control design: Computational studies for thin cylindrical shells*, Tech. Rep. CRSC-TR98-25, North Carolina State University, Raleigh, NC, June, 1998; IEEE Transactions on Automatic Control, to appear.

[6] H. T. Banks, M. Demetriou, and R. C. Smith, *Utilization of coupling effects in compensator design for structural acoustic systems – numerical examples*, Acoustical Soc. Amer., 103 (1998), pp. 872–887.

[7] H. T. Banks and K. Ito, *Approximation in LQR problems for infinite dimensional systems with unbounded input operators*, Journal of Mathematical Systems, Estimation, and Control, 7 (1997), pp. 1–34.

[8] H. T. Banks, K. Ito, and Y. Wang, *Well-posedness for damped second order systems with unbounded input operators*, Differential and Integral Equations, 8 (1995), pp. 587–606.

[9] H. T. Banks, M. L. Joyner, B. Wincheski, and W. P. Winfree, *Evaluation of material integrity using reduced order computational methodology*, CRSC Tech. Rep. 99-30, North Carolina State University, Raleigh, NC, August, 1999; Inverse Problems, submitted.

[10] H. T. Banks, Z.-H. Luo, L. A. Bergman, and D. J. Inman, *On the existence of normal modes of damped discrete-continuous systems*, CRSC-TR97-5, North Carolina State University, Raleigh, NC, February, 1997; ASME J. Applied Mechanics, 65 (1998), pp. 980–989.

[11] H. T. Banks, R. C. Smith, and Y. Wang, *Smart Material Structures: Modeling Estimation and Control*, Masson/John Wiley, Paris/Chichester, 1996.

[12] G. Berkooz, P. Holmes, and J. Lumley, *The proper orthogonal decomposition in the analysis of turbulent flows*, Annual Review of Fluid Mechanics, 25 (1993), pp. 539–575.

[13] G. Berkooz, P. Holmes, J. Lumley, and J. C. Mattingly, *Low-dimensional models of coherent structures in turbulence*, Physics Repoert-Review Section of Physics Letters, 287 (1997), pp. N4:338–384.

[14] W. L. Brogan, *Modern Control Theory*, Prentice Hall, New Jersey, 1991.

[15] R. C. H. del Rosario, *Computational Methods for Feedback Control in Structural Systems*, PhD thesis, N. C. State University, 1998.

[16] R. C. H. del Rosario and R. C. Smith, *Spline approximation of thin shell dynamics*, International Journal for Numerical Methods in Engineering, 40 (1997), pp. 2807–2840.

[17] ——, *LQR conrol of shell vibrations via piezoceramic actuators*, International Series in Numerical Mathematics, 126 (1998), pp. 247–265.

[18] ——, *LQR control of thin shell dynamics: Formulation and numerical implementation*, Journal of Intelligent Material Systems and Structures, 9 (1998), pp. 301–320.

[19] K. Fukunaga, *Introduction to Statistical Pattern Recognition*, Academic Press, New York, 1972.

[20] A. Iollo, S. Lanteri, and J. A. Désidéri, *Stability properties of POD-Galerkin approximations for the compressible Navier-Stokes equations*, INRIA Rep. de Rech. no. 3589, December, 1998; Sophia Antipolis.

[21] K. Ito and S. S. Ravindran, *A reduced order method for simulation and control of fluid flows*, tech. rep., CRSC-TR96-27, North Carolina State University, Raleigh, NC, September, 1996; Journal of Computational Physics, submitted.

[22] ——, *A reduced basis method for control problems governed by PDE*, vol. 126 of International Series in Numerical Mathematics, Birkhäuser Verlag, Basel, 1997. Also CRSC-TR97-1, North Carolina State University, Raleigh, NC, January, 1997.

[23] G. M. Kepler, H. T. Tran, and H. T. Banks, *Compensator control for chemical vapor deposition film growth using reduced order design models*, CRSC-TR99-41, North Carolina State University, Raleigh, NC, December, 1999; IEEE Trans. Semiconductor Manuf., submitted.

[24] ——, *Reduced order model compensator control of a species transport in a CVD reactor*, tech. rep., CRSC-TR99-15, North Carolina State University, Raleigh, NC, April, 1999; Optimal Control: Applications and Methods, submitted.

[25] K. Kunisch and S. Volkwein, *Control of burgers' equation by a reduced order approach using proper orthogonal decomposition*, Optimierung und Kontrolle Bericht no. 138, Universitat Graz, Austria, September, 1998; J. Opt. Theory Applic., to appear.

[26] ——, *Galerkin proper orthogonal decomposition methods for parabolic systems*, September, 1999; preprint.

[27] J. Lumley, *The structure of inhomogenous turbulent flows*, Atmospheric Turbulence and Wave Propagation, (1967), pp. 166–178.

[28] H. Ly and H. Tran, *Modeling and control of physical processes using Proper Orthogonal Decomposition*, tech. rep., CRSC-TR98-37, North Carolina State University, Raleigh, NC, November, 1998; Journal of Computational and Computer Modeling, to appear.

[29] ——, *Proper orthogonal decomposition for flow calculations and optimal control in a horizontal CVD reactor*, tech. rep., CRSC-TR98-13, North Carolina State University, Raleigh, NC, March 1998; Quarterly of Applied Mathematics, to appear.

[30] D. Nagy, *Modal representation of geometrically nonlinear behavior by the finite element method*, Computers and Structures, 10 (1979), pp. 683–688.

[31] A. Noor, *Recent advances in reduction methods for nonlinear problems*, Computers and Structures, 13 (1981), pp. 31–44.

[32] A. Noor, C. Andersen, and J. Peters, *Reduced basis technique for collapse analysis of shells*, AIAA Journal, 19 (1981), pp. 393–397.

[33] A. Noor and J. Peters, *Reduced basis technique for nonlinear analysis of structures*, AIAA Journal, 18 (1980), pp. 455–462.

[34] A. Pazy, *Semigroups of Linear Operators and Applications to Partial Differential Equations*, Springer-Verlag, New York, 1983.

[35] J. Peterson, *The reduced basis method for incompressible viscous flow calculations*, SIAM Journal on Scientific and Statistical Computing, 10 (1989), pp. 777–786.

[36] P. M. Prenter, *Splines and Variational Methods*, Wiley Classics Edition, New York, 1989.

[37] A. Pritchard and D. Salamon, *The linear quadratic control problem for infinite dimensional systems with unbounded input and output operators*, SIAM Journal on Control and Optimization, 25 (1987), pp. 121–144.

[38] L. Sirovich, *Chaotic dynamics of coherent structures*, Physica D, 37 (1989), pp. 126–145.

[39] L. Sirovich and M. Kirby, *Low-dimensional procedure for the characterization of human faces*, J. Opt. Soc. Am., 4 (1987), pp. 519–524.

[40] J. Stoer and R. Bulirsch, *Introduction to Numerical Analysis*, Springer-Verlag, New York, 1993.

[41] A. Theodoropolou, R. A. Adomaitis, and E. Zafiriou, *Model reduction for optimization of rapid thermal chemical vapor deposition systems*, IEEE Trans. Semiconductor Manuf., 11 (1998), pp. 85–98.

[42] J. Wloka, *Partial Differential Equations*, Cambridge University Press, Cambridge, 1992.

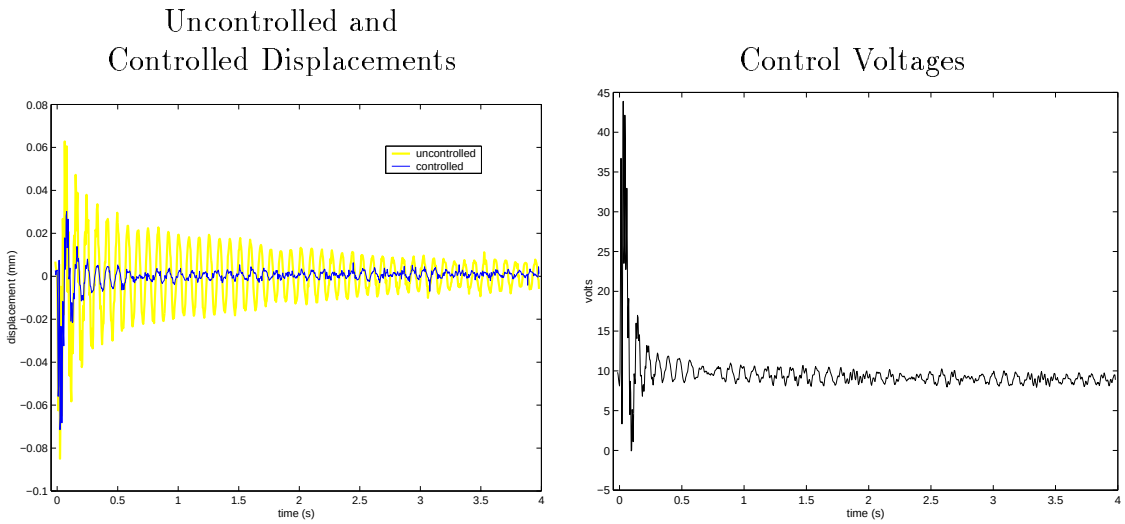

(a) Full Order

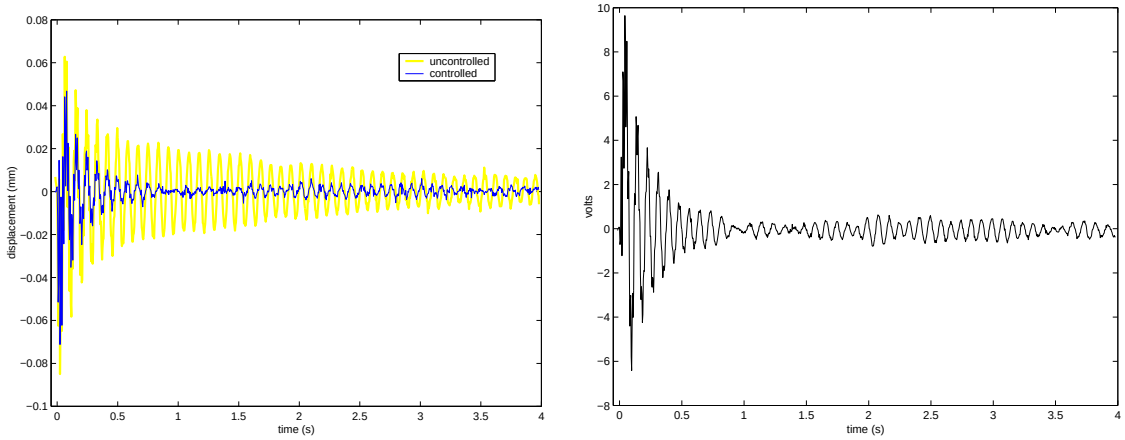

(b) 2 POD Basis Elements

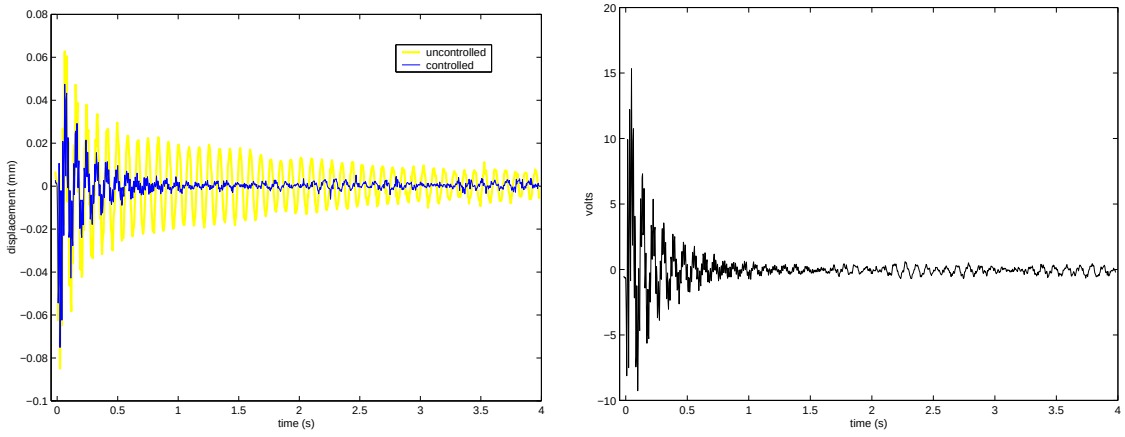

(c) 1 POD Basis Element

Figure 4: Displacements at $\hat{x} = 0.11075\ m$; (a) Full Order (b) 2 POD (c) 3 POD